
IMPROVING ADVERSARIAL ROBUSTNESS VIA PHASE AND AMPLITUDE-AWARE PROMPTING

Yibo Xu *
Xidian University
ybxu.xidian@gmail.com

Dawei Zhou *
Xidian University
dwzhou.xidian@gmail.com

Decheng Liu
Xidian University
dchliu@xidian.edu.cn

Nannan Wang †
Xidian University
nnwang@xidian.edu.cn

ABSTRACT

Deep neural networks are found to be vulnerable to adversarial noises. The prompt-based defense has been increasingly studied due to its high efficiency. However, existing prompt-based defenses mainly exploited mixed prompt patterns, where critical patterns closely related to object semantics lack sufficient focus. The phase and amplitude spectra have been proven to be highly related to specific semantic patterns and crucial for robustness. To this end, in this paper, we propose a Phase and Amplitude-aware Prompting (PAP) defense. Specifically, we construct phase-level and amplitude-level prompts for each class, and adjust weights for prompting according to the model’s robust performance under these prompts during training. During testing, we select prompts for each image using its predicted label to obtain the prompted image, which is inputted to the model to get the final prediction. Experimental results demonstrate the effectiveness of our method.

Keywords Adversarial attack · Adversarial robustness · Prompt-based defense

1 Introduction

Deep Neural Networks (DNNs) have been found to be vulnerable to adversarial noises [1, 2, 3]. This vulnerability has posed a significant threat to many deep learning applications [4, 5, 6], promoting the development of defenses [7, 8, 9, 10].

Recently, prompt-based defenses have been increasingly investigated [11, 12]. It is of interest since it does not retrain target models like adversarial training does [13, 14, 15], and does not perform major modifications on data as in denoising methods [16, 17]. However, existing prompt-based defenses mainly focus on mixed patterns, such as pixel and frequency domains (see Figure 1). These patterns cannot explicitly reflect specific patterns like structures and textures. To this end, we seek to disentangle the mixed patterns, and construct prompts for stabilizing model predictions by utilizing the specific patterns closely related to the object semantics.

The amplitude and phase spectra of the data have been proven to be able to reflect the specific semantic patterns. Previous studies indicated the amplitude spectrum holds texture patterns [18, 19], while the phase spectrum reflects structural patterns [20, 21]. Besides, cognitive sciences reveal that people tend to recognize objects by utilizing the phase spectrum [22, 23], which can also help improve the model’s generalization ability [24]. Also, the amplitude spectrum has been proven to be easily manipulated by noises and thus further processes are needed to mitigate this problem for robustness [24]. To this end, *constructing prompts using amplitude and phase spectra is expected to provide positive effects for prompt-based defenses* (see Figure 1).

*Equal contributions.

†Corresponding author.

Motivated by the above studies, we propose a *Phase and Amplitude-aware Prompting* (PAP) defense mechanism, which constructs phase and amplitude prompts to stabilize the model’s predictions during testing. We learn a phase-level prompt and an amplitude-level prompt for each class, since it can help learn more precise semantic patterns while reducing computational costs compared with learning prompts for each instance. Naturally, a question arises here: *Do amplitude-level prompts and phase-level prompts have the same effect on the model robustness?* To answer it, we utilize phase and amplitude spectra of natural examples to replace the corresponding spectra of adversarial examples respectively for testing as in Table 1. It shows phase and amplitude spectra have different effects on model’s predictions. Furthermore, we construct phase-level and amplitude-level prompts, training them under different prompting weights. Table 2 shows different weights lead to different robustness, and thus *we need to adjust their weights appropriately*.

Based on these analyses, we propose a weighting method for our prompts. Since different weights for prompting lead to different robust performances, we adjust their weights based on their influences on robustness during training. We adjust the weight for amplitude-level prompts by the ratio of accuracy under adversarial training examples with amplitude-level prompts to that with phase-level prompts, since the ratio can reflect the relative importance of amplitude-level prompts compared to phase-level prompts.

During testing, we select prompts for each image according to the model’s predicted label for it. Previous method [12] traverses all the prompts for different classes for testing, causing great time consumptions especially on datasets with many classes. To alleviate this problem, we directly select prompts for tested images according to their predicted labels. To further reduce the negative effect of mismatches between images and selected prompts, we design a loss that helps images with prompts not coming from their ground-truth labels to still be correctly classified.

Our contributions can be summarized as follows:

- Considering the amplitude and phase spectra are closely related to specific semantic patterns and crucial for robustness, we seek to design phase-level and amplitude-level prompts to provide positive gains for prompt-based defenses.
- We propose a *Phase and Amplitude-aware Prompting* (PAP) defense. Specifically, we propose a weighting method for prompts based on their impacts on the model’s robust performances for training, and propose to directly select the prompts for images based on their predicted labels for testing.
- We evaluate the effectiveness of our method for both naturally and adversarially pre-trained models against general attacks and adaptive attacks. Experimental results reveal that our method outperforms state-of-the-art methods and achieves superior transferability.

2 Related Work

2.1 Adversarial Attacks

Adversarial attacks craft malicious noises to mislead target models. White-box attacks like Projected Gradient Descent (PGD) [7], AutoAttack (AA) [25], Carlini&Wagner (C&W) [26] and Decoupling Direction and Norm (DDN) [27] craft noises through accessing and utilizing models’ intrinsic information like structures and parameters. For black-box attacks like transfer-based attacks and query-based attacks [28], attackers have no access to the models’ internal information, and thus attack only by interacting with model’s inputs and outputs.

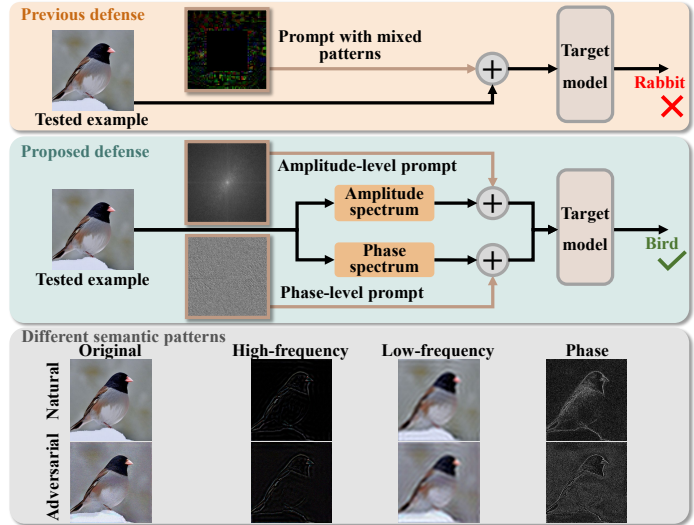


Figure 1: Differences between previous defenses and our defense. Previous method use mixed patterns like pixel or frequency domains for prompting. However, they do not explicitly focus on specific semantic patterns. The phase and amplitude spectra can reflect structures and textures specifically. Our method utilizes these specific patterns for prompting, further improving the robustness.

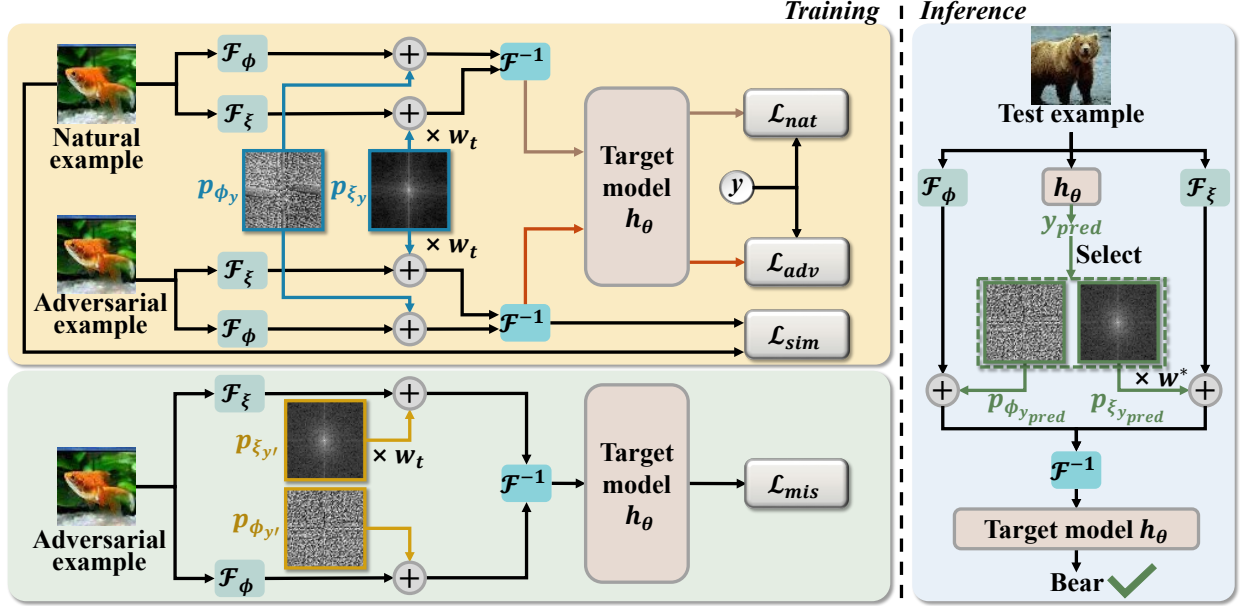


Figure 2: The framework of our method. First, We construct phase-level and amplitude-level prompts, and adjust the weights of amplitude-level prompts according to their influences on robustness for training. Then, we select prompts from predicted labels to get prompted images using the finally adjusted weights for testing.

2.2 Adversarial Defenses

Adversarial training methods (ATs) [7, 29, 30] aim at augmenting training examples through adversarial noises for training. However, ATs require modifying parameters of models and crafting noises for training, consuming significant resources. In addition, denoising methods [31, 17] purify images before feeding them into target models. It introduces an additional module for substantially modifying data to remove noises, thereby also consuming great computational resources.

To alleviate this problem, prompt-based defenses has attracted more and more interests due to its efficiency. C-AVP [12] trains pixel-level prompts for each class, and traverses all the prompts for testing. However, it requires high computation costs on datasets with numerous classes. Frequency Prompting (Freq) [11] aims at mitigating the vulnerability of models in the high-frequency domain by a masked prompting strategy. However, it does not explicitly focus on specific semantic patterns, where the semantic pattern which C-AVP focused on is also mixed (*i.e.*, the pixel domain). Differently, *we focus on specific textures and structures by prompting on the amplitude and phase spectra*. Also, our method does not traverse all the prompts for testing, *achieving superior performances efficiently through selecting prompts using predicted labels*.

3 Methodology

3.1 Preliminary

In this paper, we focus on classification tasks under adversarial settings. Given a model h_θ with parameters θ and natural data (x, y) , the adversarial example \tilde{x} is crafted for misleading h_θ . Since we focus on images, we utilize Discrete Fourier Transform (DFT) and its inverse version (IDFT), denoted as $\mathcal{F}(\cdot)$ and $\mathcal{F}^{-1}(\cdot, \cdot)$, respectively. The phase and amplitude spectra are derived as $\phi_x = \mathcal{F}_\phi(x)$ and $\xi_x = \mathcal{F}_\xi(x)$. We use ϕ_x and ξ_x to denote phase and amplitude spectra of a natural image x , while $\phi_{\tilde{x}}$ and $\xi_{\tilde{x}}$ denote the corresponding spectra of \tilde{x} . In addition, the process to recover an image from its phase and amplitude spectra is expressed as $x = \mathcal{F}^{-1}(\phi_x, \xi_x)$. *Our goal is to design prompts to assist h_θ in making accurate predictions without the need of the model retraining.*

3.2 Motivation

DNNs can be easily fooled by adversarial noises. Defenses like adversarial training and denoising methods all improve robustness with a high computational cost, promoting the development of prompt-based defenses due to the efficiency. However, existing prompt-based defenses focus on mixed patterns like pixel or frequency information, which cannot capture specific patterns like structures and textures. Thus, we seek to further disentangle these patterns for robustness.

The phase and amplitude spectra have been proven to be able to reflect specific semantic patterns. Through Fourier transform, image signals in the pixel domain can be converted into the frequency domain, which can be further decoupled into phase and amplitude spectra. The phase spectrum can reflect structures [20, 21], while the amplitude spectrum carries textures [18, 19]. Cognitive sciences indicate people tend to recognize objects by leveraging structures from the phase spectrum [22, 23], which has been proven to be able to help DNNs improve their generalization performances [24]. Also, the amplitude spectrum has been analyzed to be easily manipulated by noises, indicating the necessity to mitigate this problem for robustness [24]. *To this end, constructing phase-level and amplitude-level prompts to disentangle the mixed patterns is considered to be beneficial for improving prompt-based defenses* (see Figure 1).

3.3 Defense

Based on the above analyses, we introduce the designed *Phase and Amplitude-aware Prompting* (PAP) defense. We first construct prompts and adjust the weights of amplitude-level prompts based on their influences on robustness. During testing, we select prompts from predicted labels for prompting. The framework is shown in Figure 2.

3.3.1 Prompt Construction and Training

We firstly construct and train a phase-level prompt and an amplitude-level prompt for each class, since it can help learn precise natural semantic patterns for each class while reducing computational costs compared with learning prompts for each instance. We randomly sample a natural example x from class y , and obtain its phase spectrum $\phi_x = \mathcal{F}_\phi(x)$ and amplitude spectrum $\xi_x = \mathcal{F}_\xi(x)$ as the prompt initialization for class y . The prompt initialization for other classes is performed following the above operation. Then, the initialized phase-level and amplitude-level prompts are denoted as $\{p_{\phi_i}\}_{i=0}^{c-1}$ and $\{p_{\xi_i}\}_{i=0}^{c-1}$, where c is the number of classes. The prompted image x^p for x is obtained as follows:

$$x^p = \mathcal{F}^{-1}(\phi_x + p_{\phi_y}, \xi_x + p_{\xi_y}), \quad (1)$$

where p_{ϕ_y} and p_{ξ_y} denote the phase-level prompt and the amplitude-level prompt corresponding to the ground-truth label y of x . We perform prompting for the adversarial example \tilde{x} following the same way as Equation 1. Then, the designed training losses are introduced as follows:

Classification Loss. To enforce our prompts to stabilize the model’s predictions, we promote our prompts to learn to help correct wrong predictions of models, and thus exploit the prompted examples to construct the classification loss:

$$\mathcal{L}_{adv} = -\frac{1}{N} \sum_{i=1}^N [y_i \log(h_\theta(\tilde{x}_i^p))], \quad (2)$$

where N is the number of examples, and \tilde{x}_i^p denotes the prompted image of the adversarial example \tilde{x}_i using the prompts from its ground-truth label y_i . Then, the classification loss for the natural prompted data is presented as:

$$\mathcal{L}_{nat} = -\frac{1}{N} \sum_{i=1}^N [y_i \log(h_\theta(x_i^p))], \quad (3)$$

where x_i^p denotes the prompted image of the natural example x_i using the prompts from its ground-truth label y_i .

Reconstruction Loss. The constructed prompt could modify the phase and amplitude spectra during prompting. To ensure these modifications do not severely disrupt the original semantic patterns, we design a reconstruction loss between the prompted adversarial images and natural images as:

$$\mathcal{L}_{sim} = \frac{1}{N \times H \times W} \sum_{i=1}^N \sum_{j=1}^H \sum_{k=1}^W e^{|\tilde{m}_{j,k}^p - m_{j,k}|}, \quad (4)$$

where $\tilde{m}_{j,k}^p$ and $m_{j,k}$ denote the pixel value of \tilde{x}_i^p and the pixel value of x_i in the j -th row and k -th column respectively, and H, W denote the height and weight of the image.

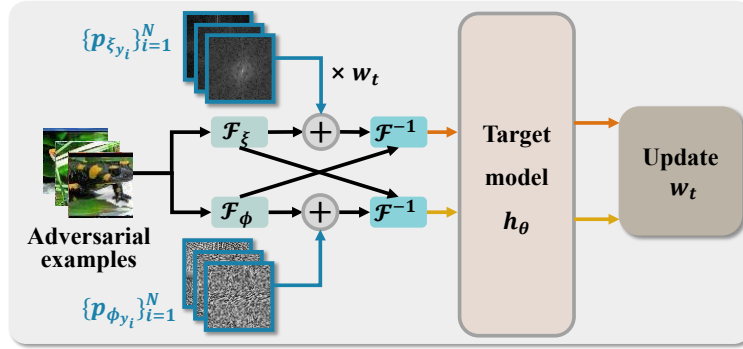


Figure 3: The weighting method for amplitude-level prompts. We use amplitude-level and phase-level prompts respectively for prompting, and adjust weights by the ratio of accuracy of images with amplitude-level prompts to that with phase-level prompts.

Data-prompt Mismatching Loss. Note that we learn a phase-level prompt and an amplitude-level prompt for each class. Also, we select prompts according to predicted labels during testing. Therefore, there exist mismatches between test images and selected prompts when testing. Previous studies [12] indicate we can get prompted images using prompts from classes different from ground-truth labels, and enforce their outputs on ground-truth labels to be larger than those on other labels, so that these images can still be correctly classified to some extent. To this end, we construct a data-prompt mismatching loss as:

$$\mathcal{L}_{mis} = \frac{1}{N} \sum_{i=1}^N \{ \max \{ h_{\theta}^{y'_i}(\tilde{x}_i^{p'}) - h_{\theta}^{y_i}(\tilde{x}_i^{p'}), -\tau \} \}, \quad (5)$$

where $\tilde{x}_i^{p'}$ is the prompted adversarial example using prompts from y'_i , which is a randomly selected label different from its ground-truth label y_i . $h_{\theta}^{y'_i}(\cdot)$ and $h_{\theta}^{y_i}(\cdot)$ denote outputs on y'_i and y_i , and τ is a threshold set as 0.1 in this paper.

3.3.2 Weighting Method

The designed prompts with the corresponding training procedure focus on helping the model make predictions accurately during testing. However, it is natural for us to question *whether the amplitude-level and phase-level prompts have the same influence on the robustness*. To this end, we conduct several experimental analyses to answer it.

We firstly replace the amplitude and phase spectra of adversarial examples with the corresponding spectrum of natural examples respectively. As shown in Table 1, for different models, the natural amplitude spectrum and natural phase spectrum contribute differently to the model’s robust performances. It indicates that *the amplitude and phase spectra have different influences on the model’s robustness*.

Due to their different influences on robustness, we may need to assign different weights for phase-level prompts and amplitude-level prompts to further improve the robustness. To show this, we assign different weights for them to obtain the prompted images for training and testing. As shown in Table 2, it is clear that different weight assignments result in different robust performances. Therefore, *we need to design a strategy which can appropriately adjust their weights*.

Based on it, we enforce prompts to assign weights for themselves according to their influences on the robustness. The robust accuracy after prompting can explicitly reflect

Table 1: The impact of different spectra on robustness. *Adv.* All denotes normal noises. *Nat. Pha./Amp.* indicate we replace phase/amplitude spectra with corresponding natural spectra.

	Adv. All	Nat. Pha.	Nat. Amp.
NAT	0.00	47.81	13.41
AT	46.82	69.00	70.10

Table 2: Robust accuracy (percentage) under different weights. α and β are weights of phase-level and amplitude-level prompts.

α	β	NAT		AT	
		None	PGD	None	PGD
1	0.01	88.82	34.44	84.31	47.69
0.01	1	91.11	5.64	73.84	50.87

Algorithm 1 Phase and Amplitude-aware Prompting (PAP).

```

1: Input: The target model  $h_\theta$ , training dataset  $\mathcal{D}$ , batch size  $n$ , the number of batches  $M$ , epoch number  $T$ , perturbation budget  $\epsilon$ ,
   the initialized phase-level prompts  $\{p_{\phi_i}\}_{i=0}^{c-1}$  and amplitude-level prompts  $\{p_{\xi_i}\}_{i=0}^{c-1}$ .
2: for  $t = 1$  to  $T$  do
3:   for  $m = 1$  to  $M$  do
4:     Read mini-batch  $\mathcal{B} = \{x_i\}_{i=1}^n$  from training set  $\mathcal{D}$ ;
5:     Craft corresponding adversarial samples  $\tilde{\mathcal{B}} = \{\tilde{x}_i\}_{i=1}^n$  at the given perturbation budget  $\epsilon$ ;
6:     Calculate  $L_{all}$  by Equation 8 to optimize  $\{p_{\phi_i}\}_{i=0}^{c-1}$  and  $\{p_{\xi_i}\}_{i=0}^{c-1}$ ;
7:   end for
8:   if  $t \bmod 5 = 0$  then
9:     update  $w_t$  via Equation 6;
10:  end if
11: end for

```

the influence of these prompts on robustness, which has been proven to be suitable for measuring the importance of them and adjusting their weights [30, 14]. *Therefore, we use the robust accuracy under these prompts to adjust their weights.* Specifically, during training, we obtain robust accuracies in training data using amplitude-level and phase-level prompts for prompting respectively. Then, the weights for amplitude-level prompts are adjusted by the ratio of accuracy under amplitude-level prompts to accuracy under phase-level prompts, since it can reflect the relative importance of amplitude-level prompts compared with phase-level prompts for robustness. The weight strategy is specified as:

$$w_t = w_{t-1} \times \frac{\sum_{i=1}^N \mathbb{I}(f(\tilde{x}_i^{p_\xi}) = y_i)}{\sum_{i=1}^N \mathbb{I}(f(\tilde{x}_i^{p_\phi}) = y_i)}, \quad (6)$$

where $\tilde{x}_i^{p_\xi} = \mathcal{F}^{-1}(\phi_{\tilde{x}_i}, \xi_{\tilde{x}_i} + w_{t-1}p_{\xi_{y_i}})$ and $\tilde{x}_i^{p_\phi} = \mathcal{F}^{-1}(\phi_{\tilde{x}_i} + p_{\phi_{y_i}}, \xi_{\tilde{x}_i})$, and y_i is the ground-truth label of the adversarial example \tilde{x}_i . $\mathbb{I}(\cdot)$ denotes the indicator function, and w_t is the weight during the t -th epoch. The Equation 1 is then incorporated with the designed weight as:

$$x^p = \mathcal{F}^{-1}(\phi_x + p_{\phi_y}, \xi_x + w_t p_{\xi_y}), \quad (7)$$

where we use Equation 7 for training, and we adjust the weight every 5 epochs for the efficiency. The finally learned weight w^* is utilized for testing, and is shown in Table 5. The weighting strategy is illustrated in Figure 3.

3.3.3 Overall Defense Procedure

To improve the overall effectiveness of our combined defense, we incorporate the the weighting strategy into the training process. The overall loss function is denoted as:

$$\mathcal{L}_{all} = \mathcal{L}_{adv} + \lambda_1 \mathcal{L}_{nat} + \lambda_2 \mathcal{L}_{sim} + \lambda_3 \mathcal{L}_{mis}, \quad (8)$$

where $\lambda_1, \lambda_2, \lambda_3$ are hyper-parameters.

The overall defense procedure is presented in Algorithm 1. Specifically, during training, for each mini-batch \mathcal{B} , we craft adversarial examples $\tilde{\mathcal{B}}$. Then, we forward-pass \mathcal{B} and $\tilde{\mathcal{B}}$ to calculate L_{all} using Equation 8, and further optimize phase-level prompts $\{p_{\phi_i}\}_{i=0}^{c-1}$ and amplitude-level prompts $\{p_{\xi_i}\}_{i=0}^{c-1}$. The weight for amplitude-level prompts is adjusted by Equation 6. Through iteratively optimizing the prompts and adjusting the weights, the prompts are expected to provide superior robustness gains.

3.3.4 Prompt Selection for Testing

After acquiring our prompts, we need to explore an effective prompt selection method during testing. Previous methods [12] traverse all the prompts from all the classes for testing on naturally pre-trained models, which sets the label with the largest output among all the prompting cases as the final prediction (see Appendix B). However, it can easily cause high computational costs for testing on large datasets with numerous classes. To address it, we promote the test image to choose prompts corresponding to its predicted label directly. Incorporated with the learned weight, we obtain the prompted image for testing as:

$$x_{test}^p = \mathcal{F}^{-1}(\phi_{x_{test}} + p_{\phi_{y_{pred}}}, \xi_{x_{test}} + w^* p_{\xi_{y_{pred}}}), \quad (9)$$

where $p_{\phi_{y_{pred}}}$ and $p_{\xi_{y_{pred}}}$ are selected prompts from the predicted label y_{pred} . Since this strategy may result in mismatches between images and selected prompts, we introduce a data-prompt mismatching loss to alleviate its negative effects on robustness, which can be seen in Section 3.3.1.

Table 3: Robust accuracy (percentage) of defenses against adversarial attacks on CIFAR-10 and Tiny-ImageNet. The target models are ResNet18 and WRN28-10. We present the most successful defense results with **bold**.

Defense	CIFAR-10 (ResNet18)				Tiny-ImageNet (WRN28-10)			
	None	AA	C&W	DDN	None	AA	C&W	DDN
None	94.83±0.05	0.00±0.00	0.00±0.00	0.00±0.00	66.62±0.11	0.00±0.00	0.00±0.00	0.02±0.00
+Freq	94.50±0.21	0.44±0.08	11.57±0.15	4.60±0.07	60.43±0.17	2.56±0.03	14.82±0.20	10.51±0.22
+C-AVP	92.67±0.51	0.61±0.11	1.93±0.07	1.05±0.17	66.52±0.02	0.39±0.00	5.83±0.07	4.19±0.25
+PAP(Ours)	87.12±0.21	37.34±0.11	80.27±0.28	66.22±0.21	57.30±0.15	5.33±0.07	42.14±0.36	33.27±0.41
AT	84.22±0.21	44.94±0.44	0.84±0.18	2.97±0.34	51.39±0.17	18.29±0.42	0.19±0.02	11.48±0.27
+Freq	78.26±0.11	51.50±0.31	35.67±0.35	35.12±0.17	44.84±0.28	22.93±0.26	19.25±0.41	21.76±0.20
+C-AVP	84.28±0.24	45.79±0.33	11.00±0.14	10.35±0.24	51.16±0.07	19.82±0.21	12.42±0.19	17.45±0.22
+PAP(Ours)	84.34±0.12	52.31±0.19	66.66±0.18	60.29±0.07	51.40±0.09	23.44±0.24	35.76±0.34	34.98±0.16
TRADES	81.59±0.21	48.98±0.23	0.74±0.10	5.03±0.09	48.98±0.07	17.87±0.07	0.15±0.00	14.29±0.09
+Freq	75.62±0.22	52.87±0.24	30.98±0.15	30.74±0.05	41.80±0.11	21.64±0.33	15.47±0.07	21.36±0.20
+C-AVP	81.58±0.17	49.44±0.24	4.47±0.20	7.97±0.35	48.59±0.19	19.15±0.34	9.18±0.17	18.57±0.13
+PAP(Ours)	81.62±0.14	54.36±0.24	63.89±0.27	57.58±0.20	48.03±0.24	22.73±0.34	30.43±0.14	31.81±0.26
MART	80.31±0.24	46.95±0.24	0.75±0.07	3.85±0.15	44.29±0.04	19.18±0.17	0.34±0.02	15.31±0.07
+Freq	74.14±0.18	52.60±0.22	34.40±0.16	32.79±0.19	37.76±0.28	22.80±0.27	15.46±0.24	21.75±0.24
+C-AVP	80.29±0.25	47.25±0.27	3.51±0.45	6.11±0.08	43.86±0.27	20.66±0.20	10.78±0.33	20.09±0.27
+PAP(Ours)	79.49±0.20	53.79±0.11	60.36±0.22	56.66±0.30	43.71±0.23	23.74±0.27	30.39±0.09	32.18±0.08

Table 4: Robust accuracy (percentage) of defenses against adversarial attacks on CIFAR-10 using the prompt selection method of C-AVP. The target model is ResNet18.

Defense	None	AA	C&W	DDN
NAT	94.83	0.00	0.00	0.00
+Freq	56.80	7.54	49.22	30.25
+C-AVP	52.17	32.26	46.78	39.51
+PAP(Ours)	86.59	38.33	83.88	70.24

4 Experiments

4.1 Experimental Settings

Datasets and Models. We use CIFAR-10 [32] and Tiny-ImageNet [33] for evaluations. CIFAR-10 has 10 classes with 50,000 training images and 10,000 testing images, and Tiny-ImageNet has 200 classes with 100,000 training images, 10,000 validation images and 10,000 testing images. All the images are normalized into $[0, 1]$. We use ResNet18 [34] and WideResNet28-10 (WRN28-10) [35] as target models, and use WRN28-10, VGG19 [36] and popular Swin Transformer [37] for evaluating the transferability.

Attack Settings. We use various attacks across two norms for evaluations. We utilize L_∞ -norm AA [25], L_2 -norm C&W [26] and L_2 -norm DDN [27]. The iteration number of L_2 -norm DDN is 20, while that of L_2 -norm C&W is 50. The perturbation budget for L_∞ -norm AA is $8/255$.

Defense Settings. We use prompt-based defenses C-AVP [12] and Freq [11] as baselines, where they are designed only for defending on naturally pre-trained models. We use natural training (NAT), AT [7], TRADES [29] and MART [30] to obtain pre-trained models. We use PGD with perturbation budget $8/255$, perturb step 10 and step size $2/255$ for training. We train prompts by SGD [38] for 100 epochs, where the initial learning rate is 0.1 and is divided by 10 at the 75-th epoch. The batch size is 512 for CIFAR-10, and 256 for Tiny-ImageNet. We set $\lambda_1 = 3$, $\lambda_2 = 400$, $\lambda_3 = 4$ for naturally pre-trained models, and $\lambda_1 = 1$, $\lambda_2 = 5000$, $\lambda_3 = 4$ for adversarially pre-trained models. We omit deviations in several tables due to their small values ($\leq 0.60\%$). More details can be found in Appendix C.

4.2 Defending against General Attacks

Defending against White-box Attacks. We apply various attacks to evaluate the robustness. The average accuracies with the deviations are presented in Table 3.

Table 5: The learned weights for the amplitude-level prompts. We show the results of ResNet18 and WRN28-10.

Model	Dataset	None	AT	TRADES	MART
ResNet18	CIFAR-10	0	0.3054	0.2572	0.3258
WRN28-10	Tiny-ImageNet	0	0.2702	0.3022	0.2848

Table 6: Robust accuracy (percentage) of defenses on different models. All the prompt-based defenses are trained on ResNet18, and then applied to the VGG19 and WRN28-10 respectively. We present the most successful defense results with **bold**.

Model	Defense	CIFAR-10				Tiny-ImageNet			
		None	AA	C&W	DDN	None	AA	C&W	DDN
VGG19	NAT	93.13	0.00	0.00	0.00	59.40	0.00	0.00	0.03
	+Freq	90.77	1.69	21.08	11.07	47.79	4.27	16.58	12.55
	+C-AVP	21.60	10.78	15.58	12.32	50.95	3.00	17.97	13.61
	+PAP(Ours)	87.65	34.28	81.33	65.65	49.30	7.39	38.66	31.26
	AT	80.12	42.61	0.38	3.42	38.99	10.73	0.13	5.40
	+Freq	73.78	49.04	34.08	33.10	30.11	15.69	16.23	16.93
	+C-AVP	79.99	43.60	10.67	10.41	38.86	14.20	16.85	16.60
	+PAP(Ours)	79.53	49.43	56.26	51.22	38.37	16.55	29.98	27.76
WRN28-10	NAT	95.42	0.00	0.00	0.00	66.62	0.00	0.00	0.02
	+Freq	94.53	0.98	18.29	7.95	54.47	3.67	18.29	13.78
	+C-AVP	10.24	9.95	10.32	10.14	61.83	2.07	19.11	13.49
	+PAP(Ours)	87.83	41.81	81.88	69.19	54.93	6.88	40.90	34.05
	AT	87.85	49.45	1.16	4.62	51.50	18.27	0.19	11.48
	+Freq	82.50	54.40	34.79	34.54	44.29	23.32	19.88	22.18
	+C-AVP	87.74	50.50	12.01	12.93	51.18	20.03	15.31	19.31
	+PAP(Ours)	87.26	54.99	70.29	63.62	51.27	23.71	36.27	35.41

Figure 4 shows our method can preserve complete semantic patterns after prompting. Quantitative analyses in Table 3 show that our method improves the robustness by a large margin on various attacks compared with existing defenses. On AutoAttack, our PAP helps increase the robust accuracy by about 37% on CIFAR-10 and 4% on Tiny-ImageNet for naturally pre-trained models, and achieves better robustness on adversarially pre-trained models from both datasets. Although Frequency Prompting improves robustness against AA for adversarially pre-trained models to some degrees, it decreases natural accuracy by about 7% on these models. On C&W and DDN, our method provides great positive effects for robustness. In addition, although our method sacrifices natural accuracy on naturally pre-trained models to some extent, it greatly improves robustness against all of these attacks (e.g., 80.27% and 42.14% against C&W on CIFAR-10 and Tiny-ImageNet).

Defending against Black-box Attacks. We apply transfer-based attacks using VGG19 as the surrogate model and query-based attack Square [28] for evaluations. Table 12 in Appendix D shows our method achieves superior performances, verifying the practicality of our defense in real scenarios.

Defenses on the Prompt Selection Method of C-AVP. To further verify the stability of our method, we use the prompt selection strategy of C-AVP on the naturally pre-trained ResNet18 on CIFAR-10 for evaluations. Table 4 shows although previous methods achieve some improvements on robustness, they reduce natural accuracy by a large margin. In comparison, our method can still protect models more effectively without losing natural accuracy too much, achieving more stable performances.

Table 7: Robust accuracy (percentage) of defenses against adaptive attacks on CIFAR-10. The target model is ResNet18.

Defense	None	AdaA20	AdaA40
NAT+Freq	94.35	0.68	0.88
NAT+C-AVP	77.74	0.01	0.01
NAT+PAP(Ours)	90.44	27.95	17.64
AT+Freq	78.30	32.44	32.22
AT+C-AVP	83.08	45.32	45.08
AT+PAP(Ours)	84.70	47.94	47.04

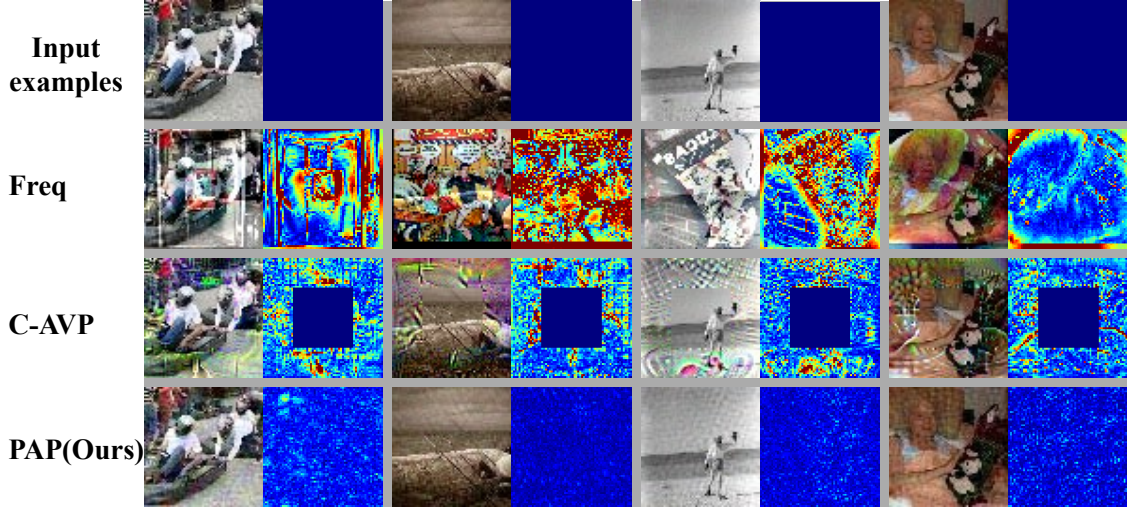


Figure 4: Visualizations of prompted images for input examples. For each pair of images, the left part denotes the prompted image, while the right part denotes the difference heatmap compared to the original input (*i.e.*, adversarial) example.

4.3 Defense Transferability

To evaluate the transferability across different models, we applied our method trained on ResNet18 to other target models, *i.e.*, WRN28-10, VGG19 and Swin Transformer. Table 6 and Table 13 (see Appendix E) show our PAP can effectively help defend against various attacks across both convolutional neural networks and vision transformers. It indicates that we can train our prompts only once and directly apply them to other models for defenses effectively.

4.4 Defending against Adaptive Attacks

Since we achieve defenses by prompting, the prompts could be leaked to attackers for performing adaptive attacks (AdaA). In this case, attackers focus on crafting adversarial noises for misleading predictions after prompting as:

$$\max_{\delta} \ell_{ce}(\mathcal{F}^{-1}(\mathcal{F}_{\phi}(x+\delta) + p_{\phi_y}, \mathcal{F}_{\xi}(x+\delta) + w_t p_{\xi_y}), y), \quad (10)$$

where ℓ_{ce} denotes the cross-entropy loss and δ is the perturbation. For fairness, we retrain our PAP on this attack and apply the same adaptive attack strategy on baselines using their own prompts to retrain them. Then, the retrained defenses are evaluated on adaptive attacks. The iteration number of attack for training is 10, while that for testing is 20 and 40. Table 7 shows our method achieves better robust accuracy, verifying the effectiveness of our method.

4.5 Ablation Studies

Loss Functions. We explore impacts of losses with different hyper-parameters. Table 8 shows removing any of these losses will damage performances, such as the extremely accuracy drop when removing \mathcal{L}_{nat} or \mathcal{L}_{mis} on NAT. Also, Appendix F shows natural and robust accuracies vary differently in various hyper-parameter settings for these losses. As a whole, the hyper-parameters we set achieve superior performances in both natural and robust accuracies.

Table 8: The impact of different losses on CIFAR-10. We report average robust accuracies due to space limitations.

Losses			NAT		AT	
\mathcal{L}_{nat}	\mathcal{L}_{sim}	\mathcal{L}_{mis}	None	Avg	None	Avg
×	✓	✓	48.27	41.35	84.32	59.77
✓	×	✓	83.64	61.56	83.20	54.19
✓	✓	×	10.01	10.43	84.34	59.48
✓	✓	✓	87.12	61.27	84.34	59.57

Table 9: The effectiveness of the weight for prompting. We report average robust accuracies on both datasets.

weight	CIFAR-10		Tiny-ImageNet	
	None	Avg	None	Avg
×	75.92	57.27	41.59	28.70
✓	84.34	59.57	51.40	31.39

Table 10: The effectiveness of learning prompts for each class on CIFAR-10 using ResNet18 compared with **universal** prompts.

Defense	None	AA	Defense	None	AA
NAT	94.83	0.00	AT	84.22	44.94
+Universal	87.54	31.81	+Universal	84.56	51.92
+PAP(Ours)	87.12	37.34	+PAP	84.34	52.31

Table 11: The effectiveness of defenses with Gaussian Blur on CIFAR-10. The target model is ResNet18.

Defense	None	AA	C&W	DDN
NAT	70.57	25.92	56.79	40.10
+Freq	70.50	26.51	57.94	40.88
+C-AVP	65.83	25.75	53.01	37.04
+PAP(Ours)	67.83	46.57	65.38	58.85
AT	78.55	55.51	57.78	54.77
+Freq	72.72	55.94	57.57	55.61
+C-AVP	78.09	55.68	59.16	55.95
+PAP(Ours)	77.01	57.41	64.57	61.68

The Weighting Strategy. To verify the effectiveness of the weighting strategy, we remove it for evaluations. As shown in Table 9, the performances drop a lot when removing the weighting strategy. Therefore, this strategy for dealing with different effects of phase-level and amplitude-level prompts on robustness is necessary and rational.

Comparison with Universal Prompts. To verify the superiority of learning prompts for each class, we train a universal phase-level prompt and a universal amplitude-level prompt for comparisons. Table 10 shows performances under universal prompts are worse than those of ours, indicating that our method helps enhance the robustness.

Effectiveness When Blurring the Edges. Some attacks like DDN tend to disrupt edges of objectives. Therefore, it’s natural to question whether robustness gains from our PAP come from edge blurring. To this end, we apply Gaussian Blur on the tested image for evaluations. As shown in Table 11, when blurring edges, our method can still achieve superior defenses, indicating the effectiveness of PAP does not come from edge blurring.

5 Conclusion

In this paper, we focus on specific semantic patterns for improving prompt-based defenses. It has been proven that phase and amplitude spectra reflect structures and textures, and both of them need to be manipulated for robustness. Therefore, we construct prompts using these spectra, and propose a Phase and Amplitude-aware Prompting (PAP) defense, which learns a phase-level prompt and an amplitude-level prompt for each class. Considering different influences of phase-level and amplitude-level prompts for robustness, we design a weighting method for them according to the robustness under these prompts. To perform testing efficiently, we select prompts according to predicted labels, and design a data-prompt mismatching loss to mitigate the negative effects of mismatches between images and their selected prompts. Experimental results demonstrate our method helps defend against general attacks and adaptive attacks, achieving superior transferability. The limitation of our work is that we sacrifice some natural accuracy when prompting on naturally pre-trained models. We will address it in the future such as using Contrastive Learning [39]. Overall, our defense explores specific semantic patterns to improve performances of prompt-based defenses.

References

- [1] Christian Szegedy, Wojciech Zaremba, Ilya Sutskever, Joan Bruna, Dumitru Erhan, Ian J. Goodfellow, and Rob Fergus. Intriguing properties of neural networks. In *International Conference on Learning Representations*, 2014.
- [2] Chaowei Xiao, Jun-Yan Zhu, Bo Li, Warren He, Mingyan Liu, and Dawn Song. Spatially transformed adversarial examples. In *6th International Conference on Learning Representations*, 2018.
- [3] Xinghao Yang, Yongshun Gong, Weifeng Liu, James Bailey, Dacheng Tao, and Wei Liu. Semantic-preserving adversarial text attacks. *IEEE Transactions on Sustainable Computing*, 8(4):583–595, 2023.

- [4] Siddharth Jaiswal, Karthikeya Duggirala, Abhisek Dash, and Animesh Mukherjee. Two-face: Adversarial audit of commercial face recognition systems. In *Proceedings of the International AAAI Conference on Web and Social Media*, volume 16, pages 381–392, 2022.
- [5] Jian-Xun Mi, Xu-Dong Wang, Li-Fang Zhou, and Kun Cheng. Adversarial examples based on object detection tasks: A survey. *Neurocomputing*, 519:114–126, 2023.
- [6] Sneha Shukla, Anup Kumar Gupta, and Puneet Gupta. Exploring the feasibility of adversarial attacks on medical image segmentation. *Multimedia Tools and Applications*, 83(4):11745–11768, 2024.
- [7] Aleksander Madry, Aleksandar Makelov, Ludwig Schmidt, Dimitris Tsipras, and Adrian Vladu. Towards deep learning models resistant to adversarial attacks. In *6th International Conference on Learning Representations*, 2018.
- [8] Jianan Zhou, Jianing Zhu, Jingfeng Zhang, Tongliang Liu, Gang Niu, Bo Han, and Masashi Sugiyama. Adversarial training with complementary labels: on the benefit of gradually informative attacks. *Advances in Neural Information Processing Systems*, 35:23621–23633, 2022.
- [9] Kai Zhao, Qiyu Kang, Yang Song, Rui She, Sijie Wang, and Wee Peng Tay. Adversarial robustness in graph neural networks: A hamiltonian approach. *Advances in Neural Information Processing Systems*, 36, 2024.
- [10] Ruiyang Xia, Dawei Zhou, Decheng Liu, Jie Li, Lin Yuan, Nannan Wang, and Xinbo Gao. Inspector for face forgery detection: Defending against adversarial attacks from coarse to fine. *IEEE Transactions on Image Processing*, 2024.
- [11] Qidong Huang, Xiaoyi Dong, Dongdong Chen, Yinpeng Chen, Lu Yuan, Gang Hua, Weiming Zhang, and Nenghai Yu. Improving adversarial robustness of masked autoencoders via test-time frequency-domain prompting. In *Proceedings of the IEEE/CVF International Conference on Computer Vision*, pages 1600–1610, 2023.
- [12] Aochuan Chen, Peter Lorenz, Yuguang Yao, Pin-Yu Chen, and Sijia Liu. Visual prompting for adversarial robustness. In *ICASSP 2023-2023 IEEE International Conference on Acoustics, Speech and Signal Processing (ICASSP)*, pages 1–5. IEEE, 2023.
- [13] Dongxian Wu, Shu-Tao Xia, and Yisen Wang. Adversarial weight perturbation helps robust generalization. *Advances in neural information processing systems*, 33:2958–2969, 2020.
- [14] Zemeng Wei, Yifei Wang, Yiwen Guo, and Yisen Wang. Cfa: Class-wise calibrated fair adversarial training. In *Proceedings of the IEEE/CVF Conference on Computer Vision and Pattern Recognition*, pages 8193–8201, 2023.
- [15] Naman Deep Singh, Francesco Croce, and Matthias Hein. Revisiting adversarial training for imagenet: Architectures, training and generalization across threat models. *Advances in Neural Information Processing Systems*, 36, 2024.
- [16] Weili Nie, Brandon Guo, Yujia Huang, Chaowei Xiao, Arash Vahdat, and Anima Anandkumar. Diffusion models for adversarial purification. *arXiv preprint arXiv:2205.07460*, 2022.
- [17] Dawei Zhou, Yukun Chen, Nannan Wang, Decheng Liu, Xinbo Gao, and Tongliang Liu. Eliminating adversarial noise via information discard and robust representation restoration. In *International Conference on Machine Learning*, pages 42517–42530. PMLR, 2023.
- [18] Trygve Randen and John Hakon Husoy. Filtering for texture classification: A comparative study. *IEEE Transactions on pattern analysis and machine intelligence*, 21(4):291–310, 1999.
- [19] Samsher Sidhu and Kaamran Raahemifar. Texture classification using wavelet transform and support vector machines. In *Canadian Conference on Electrical and Computer Engineering, 2005.*, pages 941–944. IEEE, 2005.
- [20] Peter Kovesi. Phase congruency: A low-level image invariant. *Psychological research*, 64(2):136–148, 2000.
- [21] Lin Zhang, Lei Zhang, Xuanqin Mou, and David Zhang. Fsim: A feature similarity index for image quality assessment. *IEEE transactions on Image Processing*, 20(8):2378–2386, 2011.
- [22] Jeremy Freeman and Eero P Simoncelli. Metamers of the ventral stream. *Nature neuroscience*, 14(9):1195–1201, 2011.
- [23] Evgeny Gladilin and Roland Eils. On the role of spatial phase and phase correlation in vision, illusion, and cognition. *Frontiers in Computational Neuroscience*, 9:45, 2015.
- [24] Guangyao Chen, Peixi Peng, Li Ma, Jia Li, Lin Du, and Yonghong Tian. Amplitude-phase recombination: Rethinking robustness of convolutional neural networks in frequency domain. In *Proceedings of the IEEE/CVF International Conference on Computer Vision*, pages 458–467, 2021.
- [25] Francesco Croce and Matthias Hein. Reliable evaluation of adversarial robustness with an ensemble of diverse parameter-free attacks. In *International conference on machine learning*, pages 2206–2216. PMLR, 2020.

- [26] Nicholas Carlini and David Wagner. Towards evaluating the robustness of neural networks. In *2017 IEEE Symposium on Security and Privacy (SP)*, pages 39–57. Ieee, 2017.
- [27] Jérôme Rony, Luiz G Hafemann, Luiz S Oliveira, Ismail Ben Ayed, Robert Sabourin, and Eric Granger. Decoupling direction and norm for efficient gradient-based l2 adversarial attacks and defenses. In *Proceedings of the IEEE/CVF conference on computer vision and pattern recognition*, pages 4322–4330, 2019.
- [28] Maksym Andriushchenko, Francesco Croce, Nicolas Flammarion, and Matthias Hein. Square attack: a query-efficient black-box adversarial attack via random search. In *European conference on computer vision*, pages 484–501. Springer, 2020.
- [29] Hongyang Zhang, Yaodong Yu, Jiantao Jiao, Eric Xing, Laurent El Ghaoui, and Michael Jordan. Theoretically principled trade-off between robustness and accuracy. In *International conference on machine learning*, pages 7472–7482. PMLR, 2019.
- [30] Yisen Wang, Difan Zou, Jinfeng Yi, James Bailey, Xingjun Ma, and Quanquan Gu. Improving adversarial robustness requires revisiting misclassified examples. In *International conference on learning representations*, 2019.
- [31] Guoqing Jin, Shiwei Shen, Dongming Zhang, Feng Dai, and Yongdong Zhang. Ape-gan: Adversarial perturbation elimination with gan. In *ICASSP 2019-2019 IEEE International Conference on Acoustics, Speech and Signal Processing (ICASSP)*, pages 3842–3846. IEEE, 2019.
- [32] Alex Krizhevsky, Geoffrey Hinton, et al. Learning multiple layers of features from tiny images. 2009.
- [33] Yann Le and Xuan Yang. Tiny imagenet visual recognition challenge. *CS 231N*, 7(7):3, 2015.
- [34] Kaiming He, Xiangyu Zhang, Shaoqing Ren, and Jian Sun. Deep residual learning for image recognition. In *Proceedings of the IEEE conference on computer vision and pattern recognition*, pages 770–778, 2016.
- [35] Sergey Zagoruyko. Wide residual networks. *arXiv preprint arXiv:1605.07146*, 2016.
- [36] Karen Simonyan and Andrew Zisserman. Very deep convolutional networks for large-scale image recognition. *arXiv preprint arXiv:1409.1556*, 2014.
- [37] Ze Liu, Yutong Lin, Yue Cao, Han Hu, Yixuan Wei, Zheng Zhang, Stephen Lin, and Baining Guo. Swin transformer: Hierarchical vision transformer using shifted windows. In *Proceedings of the IEEE/CVF international conference on computer vision*, pages 10012–10022, 2021.
- [38] Galen Andrew and Jianfeng Gao. Scalable training of l1-regularized log-linear models. In *Proceedings of the 24th international conference on Machine learning*, pages 33–40, 2007.
- [39] Xilie Xu, Jingfeng Zhang, Feng Liu, Masashi Sugiyama, and Mohan S Kankanhalli. Enhancing adversarial contrastive learning via adversarial invariant regularization. *Advances in Neural Information Processing Systems*, 36, 2024.
- [40] Aishan Liu, Shiyu Tang, Siyuan Liang, Ruihao Gong, Boxi Wu, Xianglong Liu, and Dacheng Tao. Exploring the relationship between architectural design and adversarially robust generalization. In *Proceedings of the IEEE/CVF Conference on Computer Vision and Pattern Recognition*, pages 4096–4107, 2023.

A Preliminary

Notation. We use capital letters like X and Y to represent random variables. Correspondingly, lower-case letters such as x and y are presented as the realizations of X and Y . We use $\mathbb{B}(x, \epsilon)$ to denote the neighborhood of x : $\{\tilde{x} : \|x - \tilde{x}\| \leq \epsilon\}$, where ϵ is the perturbation budget. Here, $\|\cdot\|$ represents the norm, which can be specified as L_∞ -norm $\|\cdot\|_\infty$ and L_2 -norm $\|\cdot\|_2$. We define $f : \chi \rightarrow \{1, 2, \dots, C\}$ as a classification function, where the f can be parameterized by a deep neural network h_θ with the parameter θ .

Problem Setting. In this paper, the task we focus on is the classification under adversarial settings, which means target models may be misled by adversarial noises. We sample natural data $\{(x_i, y_i)\}_{i=1}^n$ based on the distribution of (X, Y) , where X and Y are the variables of natural instances and their ground-truth labels. Here, $(X, Y) \in \chi \times \{1, 2, \dots, c\}$ and c is the number of classes. Given a deep neural network h_θ and a pair of natural data (x, y) , the adversarial example \tilde{x} is crafted following such a constraint:

$$h_\theta(x) \neq y \quad s.t. \quad \|x - \tilde{x}\| \leq \epsilon, \quad (11)$$

where $\tilde{x} = x + \delta$ and δ represents the adversarial noises. Since our focus is on attacking and defending for images, we utilize the Discrete Fourier Transform (DFT) and its inverse version (IDFT), denoted as $\mathcal{F}(\cdot)$ and $\mathcal{F}^{-1}(\cdot, \cdot)$, respectively. The phase and amplitude spectra are derived as $\phi_x = \mathcal{F}_\phi(x)$ and $\xi_x = \mathcal{F}_\xi(x)$. Specifically, we use ϕ_x and ξ_x to denote the phase and amplitude spectra of a natural image x , while $\phi_{\tilde{x}}$ and $\xi_{\tilde{x}}$ represent the corresponding spectra of an adversarial example \tilde{x} . In addition, the process to recover an image from its phase and amplitude spectra is expressed as $x = \mathcal{F}^{-1}(\phi_x, \xi_x)$. Our goal is to design a set of prompts to assist the classification model h_θ in making accurate predictions. These prompts are trained without the need of model retraining, and are further utilized during testing.

B Prompt Selection Method for Testing from C-AVP

C-AVP [12] aims at utilizing pixel domains for prompting. It trains a prompt for each class, and designs a prompt selection method that traverses all the prompts from all the classes to get the final predictions for testing on naturally pre-trained models especially for CIFAR-10, which can be formulated as:

$$p = p_{i^*}, i^* = \operatorname{argmax}_{i \in \mathcal{C}} h_\theta^i(x_{test} + p_i), \quad (12)$$

where p is the selected prompt for the test image x_{test} , while p_i is the prompt of class i and h_θ^i is the output of class i , and \mathcal{C} denotes the set of classes. Clearly, when the number of class becomes large, this strategy for testing can easily cause extremely high computational costs. Also, when testing using it, C-AVP indeed achieves some robustness, but sacrifices natural accuracy a lot, which can be seen in Table 4.

C Experimental Settings

Datasets and Models. In this paper, we consider two popular benchmark datasets CIFAR-10 [32] and Tiny-ImageNet [33]. CIFAR-10 has 10 classes of images with a resolution of 32×32 , which contains 50,000 training images and 10,000 testing images. The larger dataset Tiny-ImageNet has 200 classes with a resolution of 64×64 and has 100,000 training images, 10,000 validation images and 10,000 testing images. Images in all of these datasets are regarded as natural examples. We normalize all the images into the range of $[0, 1]$. Data augmentations including random crop and random horizontal flip are performed for all the data in the training stage. For the target model, we use ResNet18 [34] and WideResNet28-10 (WRN28-10) [35] for these datasets. We use WRN28-10, VGG19 [36] and a popular vision transformer architecture Swin Transformer [37] for evaluating the defense transferability across different models. The Swin Transformer is trained following previous studies about evaluating its defense performances [40].

Attack Settings. We introduce white-box attacks and black-box attacks to evaluate the defense. For white-box attack, we utilize L_∞ -norm AA [25], L_2 -norm C&W [26] and L_2 -norm DDN [27]. The iteration number of L_2 -norm DDN is set to 20, while that of L_2 -norm C&W is 50. The perturbation budget for L_∞ -norm AA is $8/255$. For L_∞ -norm C&W, the learning rate is 0.01 and the confidence is 0. All the attacks mentioned above are set as non-targeted attacks. For black-box attacks, we apply transfer-based attacks under L_∞ -norm AA, L_2 -norm DDN using VGG19 as the surrogate model and query-based attacks under Square [28]. The number of queries for Square is set to 200.

Defense Settings. We introduce two recently proposed prompt-based defenses C-AVP [12] and Freq [11] as baselines, which utilize the pixel domain and the frequency domain for prompting respectively. In addition, for the pre-trained models for optimizing and evaluating our prompts, we introduce natural training, AT [7], TRADES [29] and MART [30]. Note that all the pre-trained models are fixed without participating in any prompt training procedure. For the attack during training, we use PGD, where the perturbation budget and perturb step are $8/255$ and 10, and the step

size is 2/255. We train them using SGD [38] for 100 epochs. The initial learning rate is 0.1 with batch size 512 for CIFAR-10, and batch size 256 for Tiny-ImageNet. The initial learning rate is divided by 10 at the 75-th epoch. We set $\lambda_1 = 3$, $\lambda_2 = 400$, $\lambda_3 = 4$ for naturally pre-trained models, and $\lambda_1 = 1$, $\lambda_2 = 5000$, $\lambda_3 = 4$ for adversarially pre-trained models.

D Defending against Black-box Attacks

We perform black-box attacks under transfer-based attacks and query-based attacks. The results are shown in Table 12. It is shown that our method achieve superior robust performances under black-box settings compared with baselines.

Table 12: Robust accuracy (percentage) of defenses against black-box attacks on CIFAR-10. The target model is ResNet18, and the surrogate model is VGG19. we perform AA and DDN as the transfer-based attack strategies.

Defense	None	AA	DDN	Square
NAT	94.83	16.91	53.46	22.10
+Freq	94.50	19.37	53.85	26.43
+C-AVP	92.67	17.27	52.87	22.64
+PAP(Ours)	87.12	51.90	74.79	61.38

E Defense Transferability to Vision Transformers

We further transfer our prompts trained on ResNet18 to popular Swin Transformer for evaluating the defense transferability of our method. As shown in Table 13, our method can be transferred well to vision transformers for improving their robustness, verifying the superior transferability across both convolutional neural networks and vision transformers.

Table 13: Robust accuracy (percentage) of our prompts transferred to vision transformers. The prompts are trained on ResNet18, and the vision transformer we introduced is Swin Transformer.

Defense	None	AA	C&W	DDN
NAT	88.98	0.00	0.00	0.00
+Freq	82.77	3.47	27.55	15.50
+C-AVP	30.33	9.00	17.28	12.90
+PAP(Ours)	84.82	10.13	77.97	49.15

F Hyper-parameter Studies

We perform several ablation studies for losses with different hyper-parameters as follows. For each hyper-parameter, it varies within a certain range while other hyper-parameters are fixed. It can be seen that the natural and robust accuracies vary under different settings, and the hyper-parameters we set can achieve superior performances in both natural accuracy and robust accuracy.

G Visualizations of Prompted Images

We present additional visualized results of prompted images using our prompts, which are presented as follows. It can be seen that our method retains complete and natural semantic patterns after prompting.

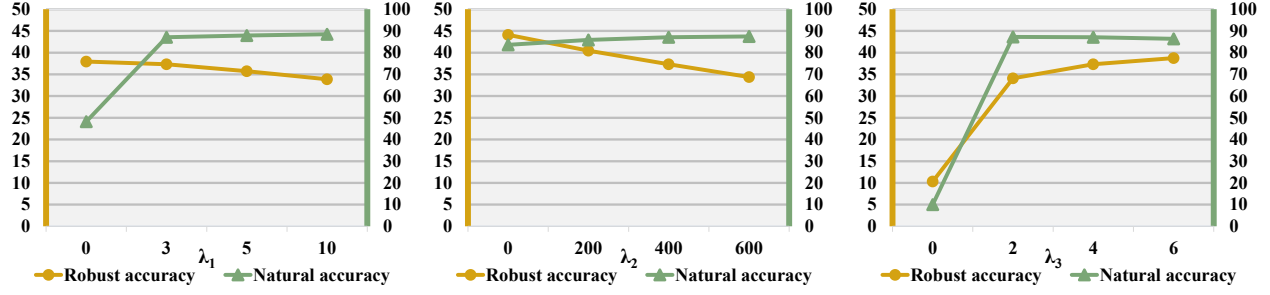


Figure 5: The impact of losses with different hyper-parameters on naturally pre-trained ResNet18 in CIFAR-10. For each hyper-parameter, it varies within a certain range while other hyper-parameters are fixed. We show the natural accuracy and robust accuracy against AA.

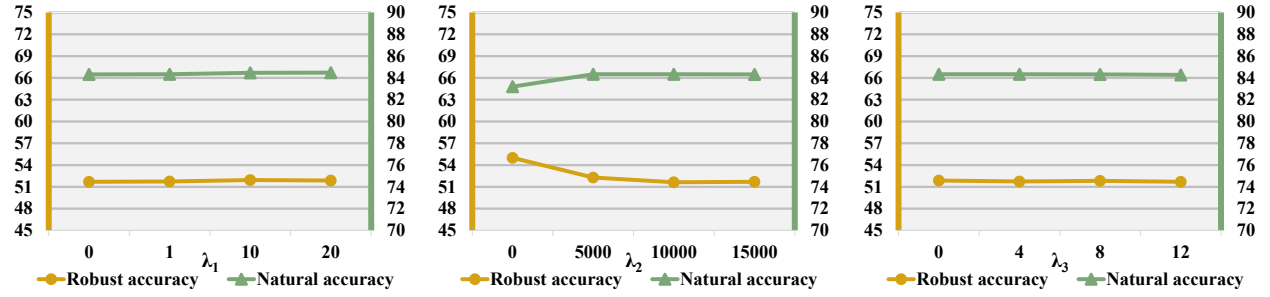


Figure 6: The impact of losses with different hyper-parameters on adversarially pre-trained ResNet18 in CIFAR-10. For each hyper-parameter, it varies within a certain range while other hyper-parameters are fixed. We show the natural accuracy and robust accuracy against AA.

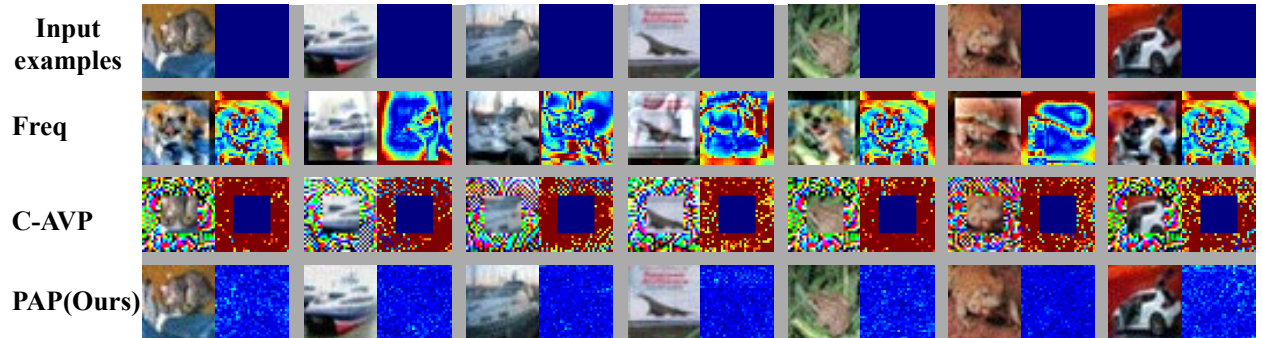


Figure 7: Visualizations of prompted images for input examples on CIFAR-10. The target model is naturally pre-trained ResNet18. For each pair of images, the left part denotes the prompted image, while the right part denotes the difference heatmap compared to the original input (i.e., adversarial) example.

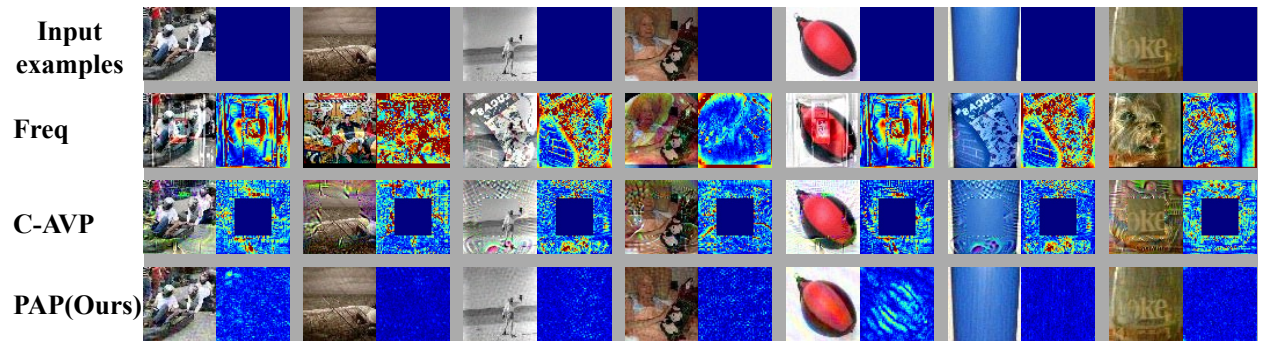


Figure 8: Visualizations of prompted images for input examples on Tiny-ImageNet. The target model is naturally pre-trained WRN28-10. For each pair of images, the left part denotes the prompted image, while the right part denotes the difference heatmap compared to the original input (*i.e.*, adversarial) example.